Nuclear and magnetic structures and magnetic properties of synthetic brochantite, Cu4(OH)6SO4

Serge Vilminot, Mireille Richard-Plouet, Gilles André, Dariusz Swierczynski, Françoise Bourée-Vigneron, Mohamedally Kurmoo

To cite this version:

Serge Vilminot, Mireille Richard-Plouet, Gilles André, Dariusz Swierczynski, Françoise Bourée-Vigneron, et al.. Nuclear and magnetic structures and magnetic properties of synthetic brochantite, Cu4(OH)6SO4. Dalton Transactions, 2006, 11 (11), pp.1455-1462. ⟨10.1039/b510545e⟩. ⟨hal-00211553⟩

HAL Id: hal-00211553

https://hal.science/hal-00211553v1

Submitted on 4 Sep 2024

Nuclear and magnetic structures and magnetic properties of synthetic brochantite, $Cu_4(OH)_6SO_4$

Serge Vilminot,*[a] Mireille Richard-Plouet,‡[a] Gilles André,[b]
Dariusz Swierczynski,[a] Françoise Bourée-Vigneron[b] and Mohamedally Kurmoo[c]

Cu4(OH)6SO4 (1) and Cu4(OD)6SO4 (2) were obtained by hydrothermal syntheses from copper sulfate and sodium hydroxide in H2O and D2O, respectively. They crystallize in the monoclinic system, space group P21/a (14), a = 13.1206(5), b = 9.8551(3), c = 6.0295(2) Å, β = 103.432(3)°, V = 758.3(1) Å3, Z = 4 and a = 13.1187(5), b = 9.8552(3), c = 6.0293(2) Å, β = 103.410(3)°, V = 758.3(1) Å3, Z = 4, respectively. They are iso-structural to the mineral brochantite and consist of double chains of edge-sharing copper octahedra that are connected to one another by corners to form corrugated planes along bc; these planes are in-turn bridged by the unprecedented μ7-sulfate tetrahedra to give a 3D-structure. All the hydrogen atoms were precisely located from refinement of the neutron powder diffraction data of the deuterated sample. Magnetic susceptibility data reveal a low-dimensional behavior at high temperature and the presence of both ferromagnetic and antiferromagnetic super-exchanges resulting in a 3D long-range antiferromagnetic ordering at 7.5 K accompanied by a small canting of the moments. The transition is confirmed by a λ-peak in the specific heat. The magnetic structure at 1.4 K shows the moments are oriented perpendicular to the corrugated planes with alternation along ±a for neighboring chains within the double chains. The enhanced incoherent scattering at low-angle suggests the existence of short-range ferromagnetic clusters.

Introduction

Natural copper hydroxysulfates are mainly formed by oxidation of copper-bearing sulfides, giving rise to antlerite, $Cu_3(OH)_4SO_4$ and brochantite, $Cu_4(OH)_6SO_4$. The key feature of their structures is the presence of edge-shared copper octahedra giving rise to infinite ribbons.[1,2] In antlerite, these ribbons are isolated and consist of three individual chains that may be regarded as a three-legged zig–zag ladder. In brochantite, named after the geologist A. J. M. Brochant de Villiers, the ribbons consist of double chains connected to one another by corners to give corrugated sheets. In each case, the sulfate tetrahedra connect the copper bearing units, either triple-chains for antlerite or sheets for brochantite. Antlerite and brochantite have also been found in the weathering patina developing on the Statue of Liberty giving it the characteristic green coloration. Successive alterations of the copper skin of the statue promote the formation of cuprite, Cu_2O, then brochantite and finally antlerite in the presence of atmospheric sulfurous gases from industrial pollution.[1] However, other reasons stimulated our interest for these copper compounds and are concerned with the synthesis, structural characterization and studies of the magnetic properties of transition metal hydroxy-sulfates.[3] In a previous paper,[4] the structure and magnetic properties of synthetic antlerite were presented, where the presence of triple-chains of copper(II) ($s = 1/2$) made such a system very exciting from a magnetic point of view. Our hopes were not disappointed since an idle spin behavior was evidenced in the magnetic structure determination from powder neutron diffraction data where the moments on the middle leg were idle and those on the outer legs were fully ordered. $Cu_4(OH)_6SO_4$, the synthetic equivalent of brochantite obtained by hydrothermal technique in a laboratory, has therefore been considered and this paper is concerned with the determination of its nuclear and magnetic structures at low temperatures and characterization of its magnetic properties by SQUID magnetometry and heat capacity.

Experimental

Synthesis

$Cu_4(OH)_6SO_4$ was prepared by hydrothermal synthesis from an aqueous suspension obtained from copper sulfate pentahydrate, $CuSO_4\cdot 5H_2O$ (4.99 g, 20 mmol)) and sodium hydroxide, NaOH (1.2 g, 30 mmol)) in 40 ml H_2O; that is in molar proportions $Cu/Na/H_2O = 1/1.5/111$. The reaction was performed under autogenous pressure in Teflon-lined stainless steel bombs of

---

a Groupe des Matériaux Inorganiques, IPCMS, CNRS-ULP UMR-7504, 23 Rue du Loess, BP 43, 67034 Strasbourg Cedex 02, France. E-mail: vilminot@ipcms.u-strasbg.fr; Fax: +33 3 88 10 72 47; Tel: +33 3 88 10 71 28
b Laboratoire Léon Brillouin, CEA-CNRS, CEA Saclay, 91191 Gif sur Yvette Cedex, France
c Laboratoire de Chimie de Coordination Organique, CNRS-UMR7140, Tectonique Moléculaire du Solide, Université Louis Pasteur, Institut Le Bel, 4 rue Blaise Pascal, 67000 Strasbourg Cedex 01, France

Supplementary information (ESI) available: TG-DTA traces, Infrared spectra, Neutron diffraction profiles (observed and calculated) at 1.4 and 300 K, ac- and dc-susceptibilities in low applied fields, atomic positions at 300 K, interatomic distances and angles at 300 K, atomic positions and magnetic moments at 1.4 K. See End of the Article

‡ Present Address: Institut des Matériaux Jean Rouxel, 2 rue de la Houssiniére, BP 32229, 44322 Nantes Cedex 03, France

125 cm^3, and filled to *ca.* 1/3. The precursor suspension obtained by mixing copper sulfate and sodium hydroxide solutions was stirred for 1 h before sealing in the reactor that was heated at 170 °C for 1 to 4 days. The synthetic brochantite was obtained as a finely divided light green powder. Attempts to promote crystal growth by varying the experimental conditions (time, temperature, dilution) were unsuccessful. Replacing the sodium hydroxide by organic amines, 1,3-diaminpropane or methylamine, in the reaction did not improve the quality of the crystals nor did they give new crystalline phases.

Samples of **2** for powder neutron diffraction studies, were prepared using the same synthetic procedure by replacing H_2O by heavy water D_2O, in order to replace H for D as much as possible in the samples. Deuterium reduces the problem of intense background usually observed for H samples due to the high incoherent scattering factor of hydrogen.

In both cases, the powders of **1** and **2** were filtered then washed with water or heavy water followed by acetone before drying at 40 °C in air.

Characterization

Thermal analysis was performed in air by use of a TG-DTA92 Setaram apparatus, at a 3.5 °C min^{-1} heating rate. Infrared spectra were recorded on an ATI Mattson spectrometer by transmission through a KBr pellet containing 1 wt% of the compound. For transmission electron microscopy, the powder was sonicated in ethanol in order to obtain a suspension of separated microcrystals. One drop was then allowed to dry on a copper grid, on which was pre-deposited a polymer membrane. The microscope used for observation is a Topcon 002B operating at 200 kV accelerating voltage and allowing a 1.9 Å resolution.

The neutron diffraction experiments were performed at the Laboratoire Léon Brillouin (CEA Saclay) using the 3T2 and G4.1 diffractometers. Data obtained on the high-resolution powder diffractometer 3T2 (λ = 1.2252 Å, $6° < 2\theta < 126°$) were used for the refinement of the nuclear structure at 300 K and those from the multi-detector (800 cells) G4.1 (λ = 2.4266 Å) for the determination of the magnetic structure and the thermal evolution study of the low temperature patterns. Therefore, 20 diffraction patterns were recorded in the 2θ range 2°–81.9°, at different temperatures between 1.4 and 100 K. The powder sample was set in a cylindrical vanadium can and held in a liquid helium cryostat. Nuclear and magnetic structures were refined using the FULLPROF program.[5] The nuclear scattering lengths ($b_{Cu} = 0.7718 \times 10^{-12}$ cm, $b_S = 0.2847 \times 10^{-12}$ cm, $b_O = 0.5803 \times 10^{-12}$ cm, $b_D = 0.6671 \times 10^{-12}$ cm and $b_H = -0.3739 \times 10^{-12}$ cm) and copper magnetic form factors were those included in this program.

Magnetic susceptibility measurements were performed in the range 2–300 K by means of a Quantum Design MPMS-XL SQUID magnetometer. Specific heat measurements between 1.65 and 38 K were carried out with a home-built equipment using a quasi-adiabatic method.

Results

Synthesis

$Cu_4(OH)_6SO_4$ has been reproducibly obtained as a fine green powder by a hydrothermal technique whereas using the same method under different conditions $Cu_3(OH)_4SO_4$ crystallizes as needle-like dark green single crystals. If the sodium hydroxide quantity is slightly increased, the color of the powder turns to blue–gray and the PXRD reveals the concomitant presence of copper oxide CuO. The modification of the other synthesis parameters (temperature, time, dilution) does not promote growth of single crystals and furthermore, the use of organic amines neither improve the quality of the crystals nor result in other phases.

Structural characterization

Powder X-ray diffraction pattern, corresponding to that of JCPDS file 87–0454, of the sample prepared from sodium hydroxide confirms the formation of only brochantite, $Cu_4(OH)_6SO_4$. When amines are used, the nature of the products prepared at 170 °C depend on the amine/Cu ratio . When DAP/Cu $\leq$ 0.5 (DAP is 1,3-diaminopropane), antlerite, $Cu_3(OH)_4SO_4$, is obtained; brochantite appears for DAP/Cu = 0.75 and a mixture of brochantite and Cu_2O for DAP/Cu = 1. In the case of MA (MA is methylamine), a mixture of antlerite and brochantite is obtained when MA/Cu $\leq$ 0.75 and pure CuO is obtained for MA/Cu = 1. Therefore, no new phase containing amine is obtained under these conditions.

Thermal analysis

The TGA reveals weight losses within two broad steps (Fig. S1 in ESI†), the first one between 265 and 435 °C is associated to the departure of water coming from the OH groups according to:

$$Cu_4(OH)_6SO_4 \rightarrow 3CuO + CuSO_4 + 3H_2O$$

and the second one between 615 and 740 °C is related to the decomposition of sulfate into oxide according to:

$$3CuO + CuSO_4 \rightarrow 4CuO + SO_3$$

The expected and observed values for both weight losses agree within *ca.* 1%. On the DT trace, two endothermal effects associated with the steps described above are observed as well as an unexpected sharp exothermal one with its maximum at 515 °C. X-Ray diffraction analysis performed on a sample previously heated at 550 °C for 2 h reveals the presence of copper oxysulfate, Cu_2OSO_4, according to JCPDS file 78–0612 and copper oxide CuO. If annealing is performed at 450 °C under the same conditions, copper oxide is evidenced and the high background level suggests the presence of an amorphous phase. Therefore, the exothermal effect at 515 °C can be attributed to the crystallization of copper oxysulfate.

Infrared spectroscopy

For the hydrogenated compound (**1**), the infrared spectrum (Fig. S2†) reveals the presence of four families of bands centered around 3400, 1100, 850 and 600 cm^{-1}. As the bands related to the O–H vibrations are shifted to lower energies upon substitution of H with D, we can, therefore, clearly identify the first and third families as those related to OH vibrations. Five bands and one shoulder appear between 3600 and 3200 cm^{-1}. While the first two at 3586 and 3562 cm^{-1} are very sharp, the remaining four at 3400, 3382, 3372 (sh) and 3268 cm^{-1} are much broader. According to Nakamoto,[6] these bands can be attributed to OH stretching vibrations. For the deuterated compound (**2**) (Fig. S2†), the above mentioned bands have nearly disappeared and have been shifted to the range 2700 to 2400 cm^{-1}, *i.e.* with a ratio ν_{OD}/ν_{OH} close to $(18/17 \times 2)^{1/2}$. The bands at *ca.* 850 cm^{-1} also disappear in the deuterated compound and can be attributed to OH libration modes. On the other hand, the bands around 1100 and 600 cm^{-1} are not affected by the H/D exchange and are attributed to the ν_3 and ν_4 vibrations of the sulfate group.

Electron microscopy

In the absence of large crystals for an X-ray structure determination and to study the homogeneity and structure of the compound we have performed transmission electron microscopy. Several crystallites were examined and found to belong to the same structure and one was selected for further study. It was oriented with respect to the incident electron beam of the TEM apparatus and further analysis reveals that this orientation could be attributed to the [100] zone axis. Due to the large parameter along *a*, the ($h\,k\,0$) Bragg reflections with $h = 1$ belonging to the first order Laue zone are visible on the experimental diffraction pattern. This particular zone-axis could be easily recorded on different crystals indicating that the platelet crystals preferentially grow along the *b* and *c* crystallographic axes. High-resolution images could be obtained along this zone-axis, as depicted in Fig. 1. First of all, the crystallites are single crystals although the edges of the crystallites appear as amorphous zones. This 10–15 nm thick amorphous layer is not due to irradiation damage since it is present on all the crystallites studied and most importantly, at the beginning of the observation. This suggests that the crystals grow from an amorphous phase under the hydrothermal conditions and at the end of the reaction the thin amorphous phase is still present at the surface.

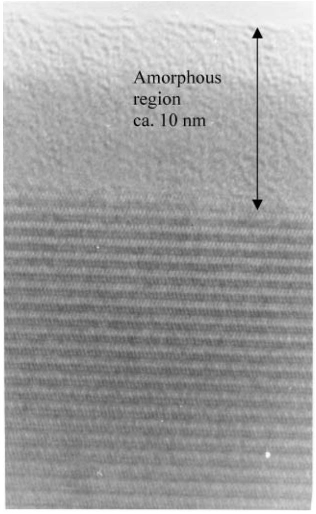

Fig. 1 A HR-TEM view of a brochantite crystal showing the layers capped by an amorphous layer of *ca.* 10 nm thickness.

Structure description

Refinement of the neutron powder data recorded at 300 K has been performed starting from the atomic coordinates of the X-ray analysis performed on a natural single crystal by Helliwell and Smith.[2] If the usual factors of merit converge to reasonable values (Table 1), the standard deviations of the atomic positions (Table S1, ESI†) and consequently, those of the bond lengths and angles (Tables 2 and S2†) are a little larger than usual, particularly for the z/c values along the short 6.029 Å axis. An explanation could be a lack of resolution with a high number of parameters due to the low symmetry with all (21) atoms in general positions. However, the final positions are in reasonable agreement with the values obtained from single crystal data.[2] The positions of the hydrogen atoms proposed by these authors are confirmed. The observed and calculated neutron powder diffraction patterns are given in Fig. S3†.

The structure can be described by double chains of brucite consisting of edge-sharing octahedra connected through the corners of adjacent ones and sulfate ions. These double chains are formed by

Table 1 Crystallographic data and refinement details at 300 K and 1.4 K from neutron powder data of the deuterated compound

	300 K	1.4 K		300 K	1.4 K
System	Monoclinic		Reflexions (magnetic)		317
Space Group	$P2_1/a$ (14)		Number of parameters	101	72
a/Å	13.1187(5)	13.070(1)	R_p (%)	12.2	8.93
b/Å	9.8552(3)	9.8335(6)	R_{wp} (%)	11.8	8.26
c/Å	6.0293(2)	6.0234(4)	R_{exp} (%)	6.88	2.13
β/°	103.410(3)	103.353(9)	R_B (%)	5.66	3.38
Wavelength/Å	1.2252	2.4266	R_F (%)	3.40	3.06
2θ range, step	6–125.7°, 0.05°	2–81.9°, 0.1°	GoF (%)	2.96	
Reflexions (nuclear)	2642	155	$R_{magnetic}$ (%)		8.43

Table 2 Selected interatomic distances (Å) for deuterated brochantite at 300 K

Cu1–OH1	1.99(2)	Cu2–OH2	2.03(2)	Cu3–OH1	2.00(2)	Cu4–OH1	1.95(2)
Cu1–OH3	2.03(2)	Cu2–OH4	2.02(2)	Cu3–OH2	1.97(2)	Cu4–OH2	2.00(2)
Cu1–OH5	1.93(2)	Cu2–OH5	1.92(2)	Cu3–OH3	2.06(2)	Cu4–OH3	2.00(2)
Cu1–OH6	1.98(2)	Cu2–OH6	1.97(2)	Cu3–OH4	2.11(2)	Cu4–OH4	1.96(2)
Cu1–O1	2.36(2)	Cu2–O1	2.36(2)	Cu3–O1	2.43(2)	Cu4–OH5	2.33(1)
Cu1–O2	2.39(2)	Cu2–O2	2.39(2)	Cu3–O3	2.41(2)	Cu4–O4	2.42(2)
⟨Cu1–O⟩	2.11	⟨Cu2–O⟩	2.12	⟨Cu3–O⟩	2.16	⟨Cu4–O⟩	2.11

Table 3 Hydrogen bonding in brochantite from neutron powder diffraction data at 300 K on a deuterated sample

	D–OD/Å		D···O/Å		OD–D···O/°
D1–OD1	0.99(2)	D1···O2	1.88(2)	OD1–D1···O2	148(5)
D2–OD2	0.95(2)	D2···OH6	1.93(2)	OD2–D2···OH6	168(10)
D3–OD3	1.00(2)	D3···O4	2.07(2)	OD3–D3···O4	154(6)
D4–OD4	0.89(2)	D4···O3	2.07(2)	OD4–D4···O3	149(6)
D5–OD5	0.99(2)	D5···O3	2.14(2)	OD5–D5···O3	132(3)
		D5···O4	2.36(2)	OD5–D5···O4	132(3)
D6–OD6	0.88(1)	D6···OH5	2.41(2)	OD6–D6···OH5	165(9)
		D6···O3	2.44(2)	OD6–D6···O3	120(3)

nearly linear chains of copper octahedra with Cu–Cu–Cu angles of 178° and 179° connected to each other by edge-sharing to give rise to double chains as found for $Zn(OH)NO_3{\cdot}H_2O$.[7] The zig–zag double chains consist of fused single chains of Cu1–Cu2 and Cu3–Cu4. These double chains are then connected to one another by corner sharing to give corrugated sheets roughly parallel to the *bc*-plane (Fig. 2); the sheets being connected to each other through the sulfate groups (Fig. 3). While the octahedra are edge-shared inside the individual chain and the double chain, they are corner-shared between double chains and may have considerable consequence on the magnetic interactions going from ferromagnetic to antiferromagnetic. As usually observed in the case of copper(II) salts, Jahn–Teller distortion promotes the formation of a (4 + 2) environment, with four short Cu–O bonds ($\langle$Cu–O$\rangle$ = 2.00 Å) and two long ones ($\langle$Cu–O$\rangle$ = 2.39 Å). The sulfate group deviates from a regular tetrahedral symmetry but this result is related to some imprecision due to neutron powder diffraction from the sulfur atom having a rather low cross-section. From single crystal X-ray data, the sulfate group is nearly regular with S–O bond lengths between 1.480(6) and 1.489(6) Å. This study also confirms the location of the hydrogen/deuterium atoms proposed by Helliwell and Smith,[2] with O–D distances varying between 0.88(1) and 1.00(2) Å, the shortest ones (D4 and D6) corresponding to positions with the greatest proportion of H. These atoms are involved in single deuterium bonds for D1 to D4 and in bifurcated deuterium bonds for D5 and D6 (Table 3).

The sulfate group presents an interesting coordination with the surrounding metals (Fig. 4). It is covalently bonded to seven copper atoms, O1 to three, O2 to two and O3 and O4 to one each. The O–O distances are normal and range between 2.363 and 2.427 Å. However, the Cu–O–S angles deviate from the tetrahedral angle and lie within the range 103 to 139°.

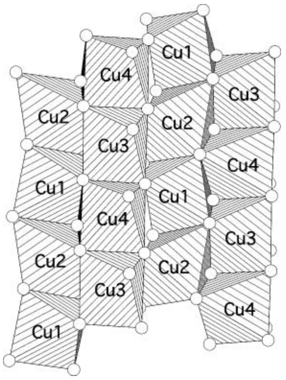

Fig. 2 View of a layer showing the edge-sharing double-chains of brucite connected by the apices of the octahedral of neighbouring double-chains.

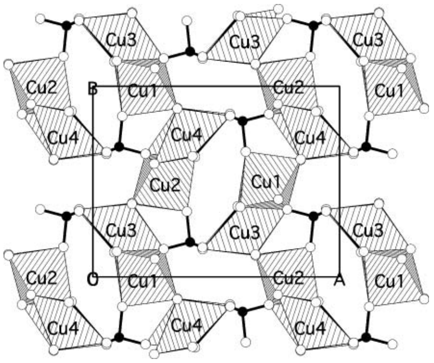

Fig. 3 View of the structure along the *c*-axis showing the connections of the double-chains into layers bridged by the sulfate groups.

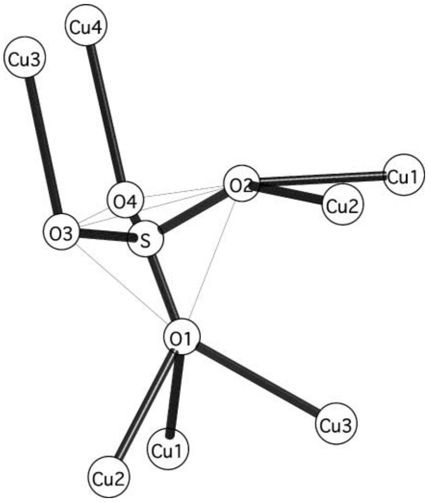

Fig. 4 The coordination of the sulfate group showing the seven bonded copper atoms.

Magnetic properties

The magnetic susceptibility of **1** measured in an applied field of 100 Oe is shown in Fig. 5. It is characterized by three temperature-regions. For $T > 50$ K, the ZFC-FC susceptibility is reversible and shows a broad maximum centered at 60 K. Below 50 K, there are two bifurcations at 18 and 7 K observed in ZFC-FC data. Analysis of the data above 150 K to the Curie–Weiss law, $\chi = C/(T - \theta)$, gives $C = 2.002(8)$ (1) emu K mol^{-1} and $\theta = -90(1)$ K. Using $C = Ng^2\mu_B{}^2s(s + 1)/3k$ we obtain $g = 2.311(9)$ in fair agreement

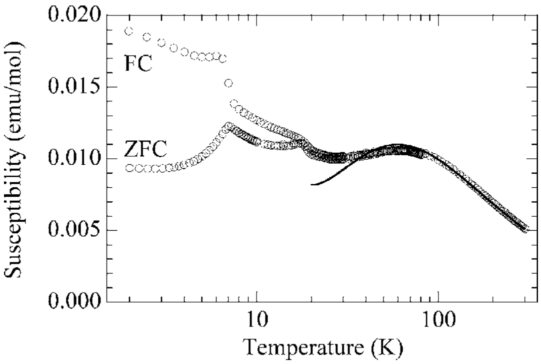

Fig. 5 Magnetic susceptibility measured in an applied field of 100 Oe including ZFC/FC data for the temperature region 2–80 K. The solid line is the theoretical simulation of a Quadratic layer antiferromagnet with $J/k = -65$ K and $g = 2.25$.

with those for Cu(II). The negative θ value points to strong and dominant antiferromagnetic interaction. The broad maximum at 60 K can be attributed to short-range low-dimensional antiferromagnetic behavior within the layer. By close examination of the crystal structure within a layer and not considering interactions between layers, we can assign six independent exchange pathways (J_{12}, J_{13}, J_{14}, J_{23}, J_{24}, J_{34} where J_{ij} is the interaction between Cu(i) and Cu(j)) between the nearest neighbor copper centers within one double chain and four (J'_{13}, J'_{14}, J'_{23}, J'_{24}) between neighboring double chains. It is clear from the data that these parameters are not tractable as they are also related to one another. Two approximate models for the magnetic properties are the quadratic (QLAF) and triangular (TLAF) layer antiferromagnets. A theoretical calculation for the QLAF is shown in Fig. 5 for a J/k of -65 K and using $g = 2.25$.[8] This model is strictly applicable to $s = 1/2$ moment carriers arranged on a square lattice with one exchange constant between sites. The analytical function is only valid for $kT > J/2$. Both of these values are reasonable considering those found from the Curie–Weiss fit. Below 50 K, the two bifurcations suggest two long-ranged orderings. From the neutron data (see later) the one at 7 K appears to be intrinsic to the compound. Below 25 K, the slight increase of the susceptibility suggests a weak ferromagnetic component within the layer starts to come into play as $kT \approx J_F$. Three-dimensional long-range magnetic ordering sets in at 7 K *via* weak antiferromagnetic super-superexchange through the sulfate. To confirm the presence of a spontaneous magnetization, we measured the dc-magnetization in a field of 2 Oe after zero-field cooling (Fig. S4†). Again the bifurcations at the two transitions are evident. However, none of them show any imaginary component of the ac-susceptibilities. Isothermal magnetizations above and below the transition at 7 K are featureless showing a linear dependence with field. The magnetizations in field of 50 kOe are only a fraction of that expected if all the moments were aligned in the direction of the applied field. We also note that the value at 2 K is less than that at 10 K. These observations are consistent with those expected for a canted-antiferromagnet.

Specific heat

The temperature dependence of the specific heat (Fig. 6) shows a characteristic λ-type anomaly with a peak at 6.3 K, confirming a phase transition towards a 3D ordered state. Attempts to extract the magnetic contribution of the specific heat from the total and to estimate the entropy was unsuccessful. After deducing the phonon contribution as a AT^3 and assuming the magnetic contribution adopts a T^{-2} term did not give a reliable result. However, such an analysis results in an estimated entropy of 7.9 J K^{-1} mol^{-1}, which is far from the expected 4 × 5.76 J K^{-1} mol^{-1}. This deviation may be attributed to magnetic contribution from the low dimensional correlations giving rise to the broad maximum centered at *ca.* 55 K observed in the susceptibility measurements.

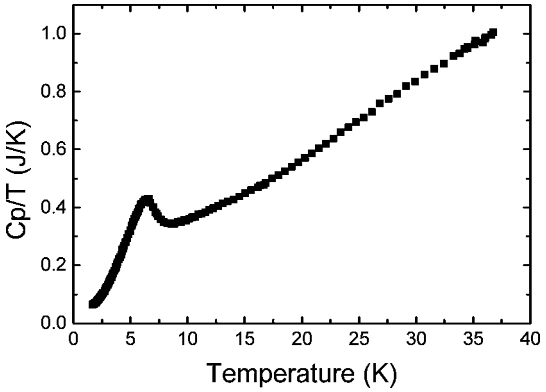

Fig. 6 Temperature dependence of the specific capacity normalized to the temperature.

Magnetic structure

The comparison of the diffraction patterns recorded at 1.4 and 12 K, *i.e.* below and above the 3D-magnetic ordering reveals only minor differences. A zoom of the intensity in the 2θ-range between 10 and 35° only evidences two clear features, at around 18° and 30.7° and corresponding to (110) and (120) planes, respectively. Moreover, the intensities of the two features are very small and one would, therefore, expect low values for the associated copper magnetic moments. The second observation concerns the evolution of the background at a low diffraction angle over the whole explored temperature domain (Fig. 7). The diffusion signal first decreases between 100 and 55 K, then increases to reach a plateau below 40 K, finally decreasing down from 12 to 1.4 K. This behavior is characteristic of the formation of ferromagnetic clusters.

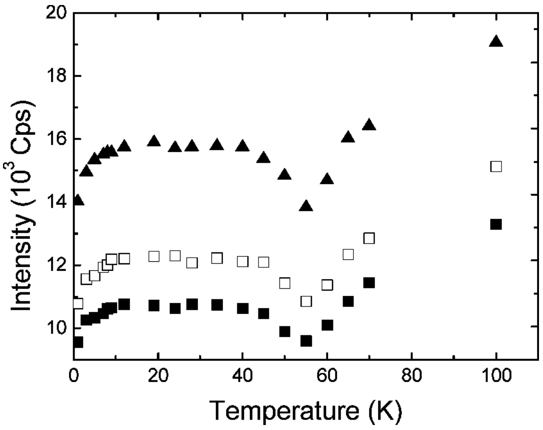

Fig. 7 Evolution of the background at low diffraction angles *versus* temperature for 2θ values of 2.3, 2.4 and 2.5° (from top to bottom).

The magnetic structure has been studied from neutron powder diffraction data collected at eight temperatures ranging between 1.4 and 12 K. We determined the associated magnetic structure with the help of Bertaut's representation analysis method,[9] applied to $P2_1/a$ space-group, $k = (0\ 0\ 0)$ propagation vector and (4e) Wyckoff positions for all copper ions. Four one-dimensional irreducible representations (IR) are evidenced, Γ_1 to Γ_4, which are associated to basis vectors (magnetic structures) for the copper ions.[10] Consideration of the nuclear structure reveals that Cu1 and Cu2 on one hand, and Cu3 and Cu4 on the other belong to different chains within the ribbons. Therefore, it is reasonable to consider that inside a chain the same model must be applied with the same magnetic moments on Cu1 and Cu2 or Cu3 and Cu4. It clearly appears that the Γ_4 solution applied for both kinds of chains gives a much better agreement between observed and calculated intensities of the magnetic lines with a merit factor at least two times smaller than for the other models. The magnetic components of the copper ions have significant values only along the *a*-axis. Consequently, the refinement of the nuclear positions (Table S3†) and magnetic vectors of the copper atoms from the 1.4 K data (Fig. S5†) using this model results in a magnetic structure (Fig. 8) in which the two kinds of chains, around Cu1 + Cu2 and Cu3 + Cu4, exhibit a ferromagnetic order and are antiferromagnetically coupled to one another. The magnetic moment on Cu1 and Cu2 ions is quite small, 0.22(11) μ_B, but a refinement with a zero value on these ions yields a significant increase of the figure of merit from 8.43 to 12.9%. The magnetic moment for Cu3 and Cu4 ions is significantly higher, 0.74(7) μ_B, but still lower than the expected 1 μ_B (Table S4†).

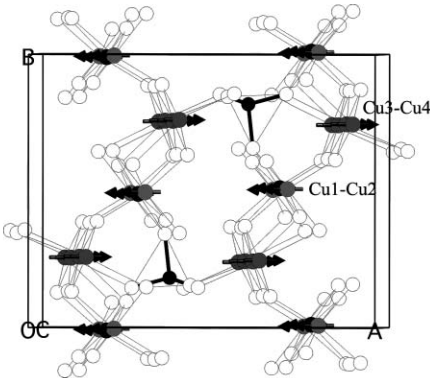

Fig. 8 Orientation of the magnetic moments as determined from analysis of the neutron data.

Discussion

In the $Cu(OH)_2$–$CuSO_4$ system, only two phases have been obtained for a variety of hydrothermal synthetic conditions, antlerite $Cu_3(OH)_4SO_4$ and brochantite, $Cu_4(OH)_6SO_4$. The hydrated minerals related to brochantite, posnjakite $Cu_4(OH)_6SO_4.H_2O$, wroewolfite and langite $Cu_4(OH)_6SO_4.(H_2O)_2$ have not been evidenced in our study. This may mean that hydrothermal synthesis cannot reproduce the natural conditions for mineral formation.

Table 4 Tentative assignments of the O–H(D) stretching modes for H and D brochantites. Related interatomic distances (Å)

	ν(OH)[a]	ν(OD)[a]	D···O/Å	O
OH(D)1	3267	2436	1.88(2)	O2
OH(D)2	3372 (sh)	2497 (sh)	1.93(2)	OH6
OH(D)3	3382	2516	2.07(2)	O4
OH(D)4	3399	2524	2.07(2)	O3
OH(D)5	3562	2634	2.14(2)	O3
			2.36(2)	O4
OH(D)6	3586	2647	2.41(2)	OH5
			2.44(2)	O3

[a] In cm^{-1}.

The knowledge of the deuterium atomic positions (Table S1†) allows one to propose assignments of the OH and OD stretching vibration bands, which were tentatively performed by Schmidt and Lutz on the basis of the O···O distances.[11] According to D···O distances, D6 defines a very weak bifurcated D bond and can be related to the band with the highest energy, 2647 cm^{-1}. The other sharp band at 2634 cm^{-1} can be assigned to D5 defining again a bifurcated D bond. The other vibration bands have been assigned with decreasing energy related to shorter D···O distances. It is interesting to mention that the 2524 and 2516 cm^{-1} vibration bands that are very close to each other can be assigned to D3 or D4 for which D···O distances are the same (2.07 Å). The results are summarized in Table 4.

The proposed magnetic structure in the ordered state agrees well with the results of magnetic susceptibility. Both corrugated planes containing copper ions exhibit an antiferromagnetic ground state, but it appears that interactions of opposite signs concur to the overall behavior. Thus, the magnetic moments of the copper atoms inside the individual Cu1 + Cu2 and Cu3 + Cu4 chains order ferromagnetically and are aligned antiparallel to each other within the sheet, all the magnetic moments pointing in a direction roughly perpendicular to the plane. Above T_N, a broad maximum in the susceptibility is evidenced at *ca.* 55 K and has been attributed to in-plane short-range antiferromagnetic interactions that compete with weak ferromagnetic interactions to result in a rise just before the 3D long-range antiferromagnetic transition. On the other hand, the presence of an enhanced background at low angles in the neutron powder data may indicate the presence of ferromagnetic clusters or chains, which appear along the plateau between 40 and 12 K. Therefore, it appears possible that individual chains (Cu3 + Cu4) couple ferromagnetically (the extension of ordering cannot be evaluated). The correlation length in the third dimension, resulting in the long range Néel ordering, causes the disappearance of the background below 12 K. The effect evidenced at 18 K by susceptibility measurements could correspond to a weak modification that is not detected by powder neutron diffraction.

Different papers have discussed the relation between the sign of the exchange coupling in copper(II) compounds to the bridging Cu–O–Cu angle.[12–17] In the case of antlerite $Cu_3(OH)_4SO_4$, we confirmed this relation with a cross-over around 97.5° for the bridge angle, ferromagnetic coupling appearing for lower bridge angles and AF one for higher angles.[3] Moreover, in case of double (O + OH) exchange pathways, the ferromagnetic exchange is favored by the low Cu–O–Cu value compared to the high Cu–OH–Cu value. A preliminary study of brochantite using only this concept to solve the magnetic structure does not yield the right model, differing from the one obtained in the present work starting from group theory calculations.[18] The error in

Table 5 Correlations between Cu–O–Cu angles and magnetic coupling in antlerite (upper part) and brochantite (lower part)

Cu–O–Cu	Angle/°	Angle-97/°[a]	Resultant[b]	Coupling[c]	Structure[d]
Cu1–OH3–Cu1	99.6	+2.6	+2.6	AF	AF
Cu2–O1–Cu2	76.4	−20.6	−15.66	F	F
Cu2–OH1–Cu2	101.9	+4.9			
Cu2–O2–Cu2	81.3	−15.7	−6.7	F	F
Cu2–OH2–Cu2	106.0	+9.0			
Cu1–OH1–Cu2	96.7	−0.3	+6	AF	AF
Cu1–OH3–Cu2	103.6	+6.6			
Cu1–O2–Cu2	83.3	−13.7			
Cu1–OH3–Cu2	108.9	+11.9	−1.8	F	F
Cu1–O2–Cu2	80.0	−17.0	−11.9	F	F
Cu1–OH5–Cu2	102.1	+5.1	−10.3	F	
Cu1–O1–Cu2	80.1	−16.9			
Cu1–OH6–Cu2	103.6	+6.6			
Cu3–OH1–Cu4	98.9	+1.9	+2.8	**AF**	**F**
Cu3–OH3–Cu4	97.9	+0.9	+1.4	**AF**	
Cu3–OH2–Cu4	97.3	+0.3			
Cu3–OH4–Cu4	98.1	+1.1			
Cu1–OH1–Cu3	110.7	+13.7	+4.9	AF	AF
Cu1–O1–Cu3	88.2	−8.8			
Cu1–OH1–Cu4	107.4	+10.4	+10.3	AF	AF
Cu1–OH5–Cu4	96.9	−0.1			
Cu2–O1–Cu3	87.4	−9.6	−1.5	**F**	**AF**
Cu2–OH2–Cu3	105.1	+8.1			
Cu2–OH2–Cu4	103.2	+6.2	+5.5	AF	AF
Cu2–OH5–Cu4	96.3	−0.7			
Cu1–OH3–Cu3	121.7	+24.7	+24.7	AF	AF
Cu1–OH3–Cu4	124.5	+27.5	+27.5	AF	AF
Cu2–OH4–Cu3	120.0	+23.0	+23.0	AF	AF
Cu2–OH4–Cu4	121.2	+23.2	+23.2	AF	AF

[a] Assuming the critical angle of 97° from ferromagnetic to antiferromagnetic coupling. [b] Resultant sum of angle-97 for doubly bridged Cu···Cu. [c] Assignment of coupling according to the sign of the resultant. [d] Effective coupling as determined by neutron refinement.

the interpretation was that, in the case of double exchange, the nature on the coupling depends on the relative values of the Cu–O–Cu angles. Taking into account these values through the difference between F and AF contributions allows one to explain the results obtained in the two copper compounds, antlerite and brochantite as shown in Table 5, even if for two cases (bold characters) a discrepancy is observed, both involving rather low resultant values for the angles.[3] In correlating the magnetic measurements with the magnetic structure determination, we can propose that the antiferromagnetic coupling between successive chains has the highest magnitude as it dominates the high temperature susceptibility. The second in this hierarchy would be the ferromagnetic coupling within the individual chains, which can result in the formation of ferromagnetic 2D clusters at intermediate temperatures as apparent in the neutron data. And finally, the weak antiferromagnetic interaction between the sheets *via* the sulfate anion is the smallest.

Conclusion

Hydrothermal synthesis allows synthetic brochantite $Cu_4(OH)_6SO_4$ to be obtained as a fine light green powder. Magnetic structure determination from neutron powder data proves the presence of ferromagnetic chains that are coupled antiferromagnetic to each other inside the corrugated planes, the planes being also AF coupled. All magnetic moments are aligned along the *a*-axis, *i.e.* perpendicular to the planes with values of 0.22(11) and 0.74(7) μ_B for Cu1 + Cu2 and Cu3 + Cu4 chains, respectively. The rather high values of the standard deviations result from the weak magnetic peaks. An interesting feature concerns the evidence of the formation of ferromagnetic clusters in relation with the evolution of the background at low θ. Finally, the relation between Cu–O–Cu bridge angles and the nature of the exchange coupling has been confirmed and this relation can even be used to solve the magnetic structure taking into account the relative magnitudes of the angle values.

Acknowledgements

We thank the CNRS for funding this work, E. Marino for her contribution in the early stages and A. Derory and J.-P. Lambour for technical assistance.

References

1 F. C. Hawthorne, L. A. Groat and R. K. Eby, *Can. Mineral.*, 1989, **27**, 205–209.
2 G. Cocco and F. Mazzi, *Period. Mineral.*, 1959, **28**, 121–149; M. Helliwell and J. V. Smith, *Acta. Crystallogr., Sect. C*, 1997, **53**, 1369–1371; S. Merlino, N. Perchiazzi and D. Franco, *Eur. J. Mineral.*, 2003, **15**, 267–275.
3 S. Vilminot, M. Richard-Plouet, G. André, D. Swierczynski, F. Bourée-Vigneron and M. Kurmoo, *Inorg. Chem.*, 2003, **42**, 6859–6867; M. Ben Salah, S. Vilminot, G. André, M. Richard-Plouet, F. Bourée-Vigneron, T. Mhiri and M. Kurmoo, *Chem. Eur. J.*, 2004, **10**, 2048–2057; M. Ben Salah, S. Vilminot, T. Mhiri and M. Kurmoo, *Eur. J. Inorg. Chem.*, 2004, 2272–2276; M. Ben Salah, S. Vilminot, M. Richard-Plouet, G. André, T. Mhiri and M. Kurmoo, *Chem. Commun.*, 2004, 2548–2549.
4 S. Vilminot, M. Richard-Pouet, G. André, D. Swierczynski, M. Guillot, F. Bourée-Vigneron and M. Drillon, *J. Solid State Chem.*, 2003, **170**, 255–264.

5 J. Rodriguez-Carvajal, *FULLPROF: Rietveld, profile matching and integrated intensity refinement of X-ray and/or neutron data, 3.5d version*, (1998), Léon-Brillouin Laboratory, CEA Saclay, France.

6 K. Nakamoto, *Infrared and Raman Spectra of Inorganic and Coordination Compounds*, 4th edn, Wiley-Interscience, New York, USA, 1986.

7 L. Eriksson, D. Louer and P. E. Werner, *J. Solid State Chem.*, 1989, **81**, 9.

8 M. E. Lines, *J. Phys. Chem. Solids*, 1970, **31**, 101.

9 E. F. Bertaut, *Acta Crystallogr., Sect. A*, 1968, **24**, 217.

10 (*a*) KAREP–a program for calculating irreductible space group representationsE. Hovestreydt, I. Aroyo, S. Sattler and H. Wondratschek, *J. Appl. Crystallogr.*, 1992, **25**, 544; (*b*) *BASIREPS-a Program for Calculating Non-normalized Basis Functions of the Irreductible Representations of the Little Group Gk for Atom Properties in a Crystal*, J. Rodriguez-Carvajal, Laboratoire Léon Brillouin (CEA-CNRS), CEA Saclay, Gif sur Yvette, France.

11 M. Schmidt and H. D. Lutz, *Phys. Chem. Minerals*, 1993, **20**, 27–32.

12 J. B. Goodenough, *J. Phys. Chem. Solids*, 1958, **6**, 287–297.

13 J. Kanamori, *J. Phys. Chem. Solids*, 1959, **10**, 87–98.

14 A. P. Ginsberg, *Inorg. Chim. Acta*, 1971, **5**, 45–68.

15 P. J. Hay, J. C. Thibeault and R. Hoffmann, *J. Am. Chem. Soc.*, 1975, **97**, 4884–4898.

16 V. H. Crawford, H. W. Richardson, J. R. Wasson, D. J. Hodgson and W. E. Hatfield, *Inorg. Chem.*, 1976, **15**, 2107–2110.

17 H. Weihe and H. U. Güdel, *J. Am. Chem. Soc.*, 1998, **120**, 2870–2879.

18 S. Vilminot, M. Richard-Plouet, G. André, D. Swierczynski, F. Bourée-Vigneron, E. Marino and M. Guillot, *Cryst. Eng.*, 2002, **5**, 177–186.

Supplementary Information

Nuclear and Magnetic Structures and Magnetic Properties of Synthetic Brochantite, $Cu_4(OH)_6SO_4$

Serge Vilminot,* [a] Mireille Richard-Plouet,† [a] Gilles André,[b] Dariusz Swierczynski,[a] Françoise Bourée-Vigneron,[b] and Mohamedally Kurmoo [c]

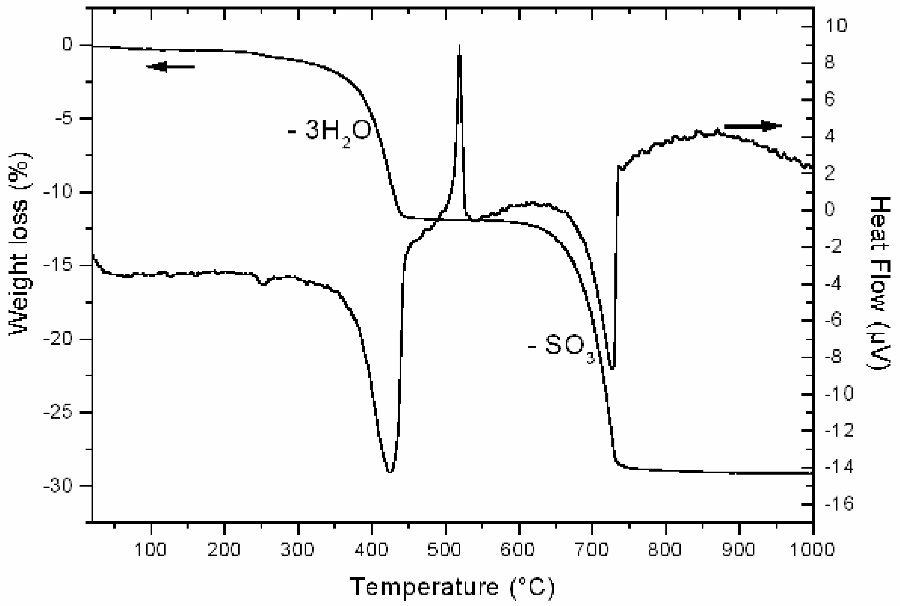

Figure S1: TG-DTA traces recorded under air at a 3.5°C/mn heating rate

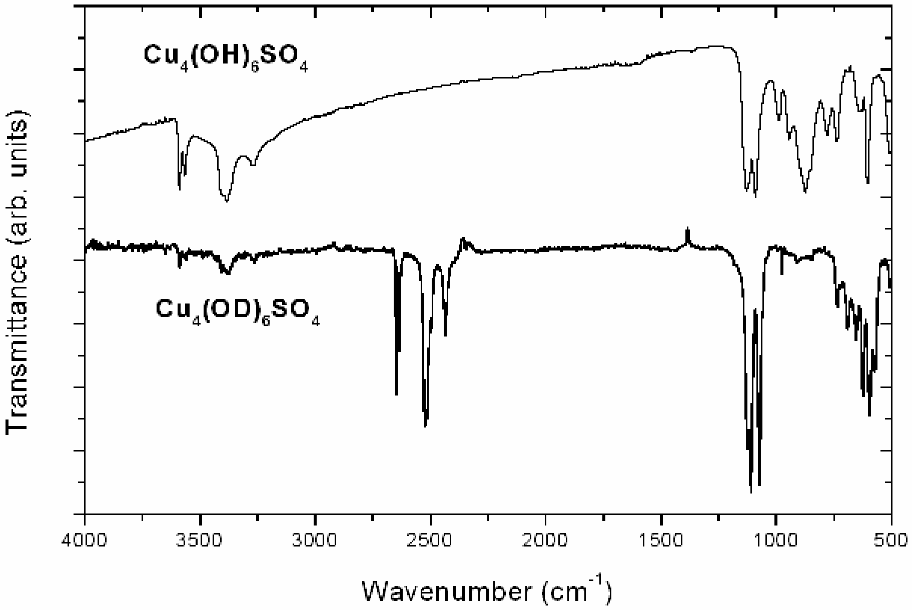

Figure S2: Infrared spectra of a) $Cu_4(OH)_6SO_4$ and b) $Cu_4(OD)_6SO_4$

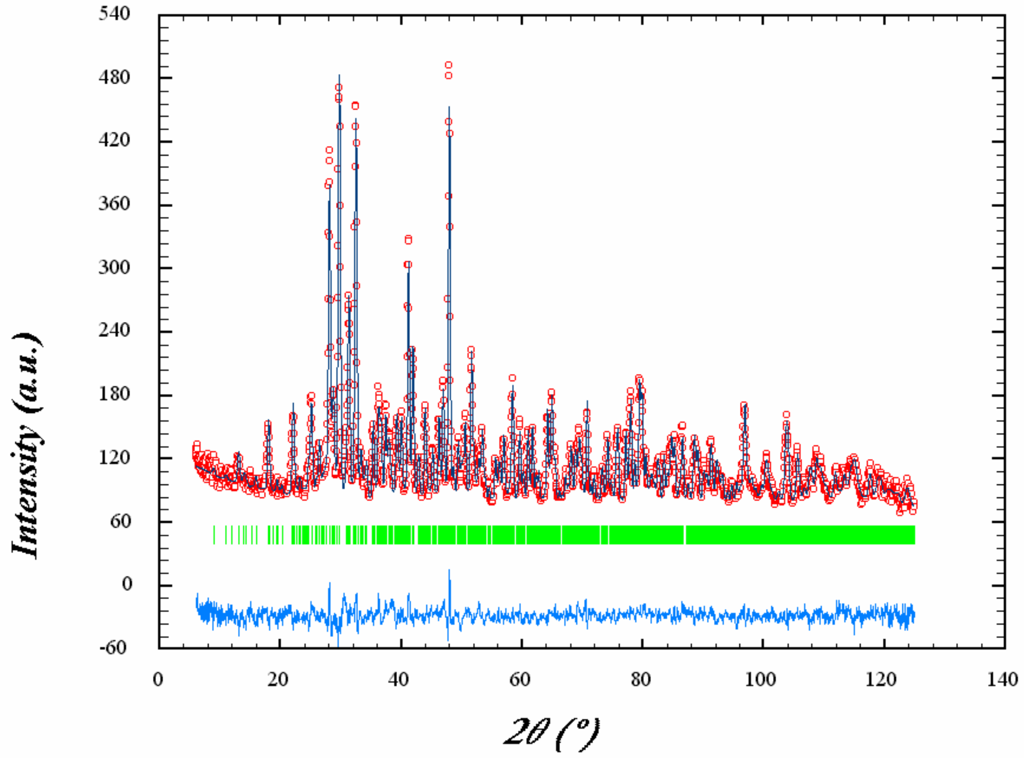

Figure S3. Observed (O) and calculated (──) profiles of the powder neutron pattern of $Cu_4(OH)_6SO_4$ obtained on the 3T2 diffractometer at 300 K with position of the Bragg reflections (short vertical lines) and difference between observed and calculated profiles.

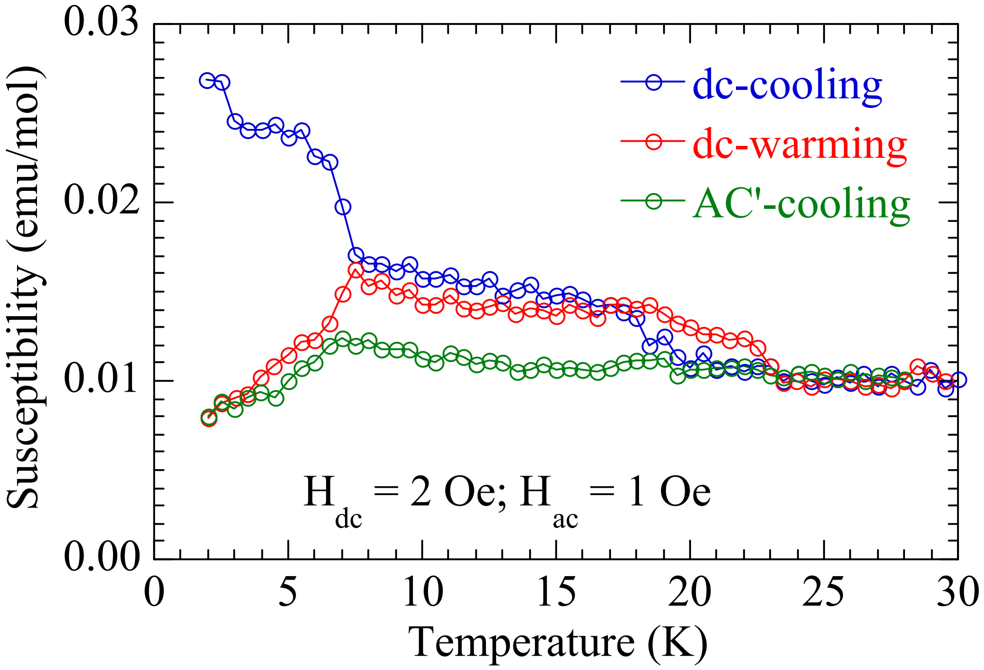

Figure S4. ac- and dc-susceptibilities measured in low applied fields (H_{ac} = 1 Oe (17 Hz), H_{dc} = 2 Oe).

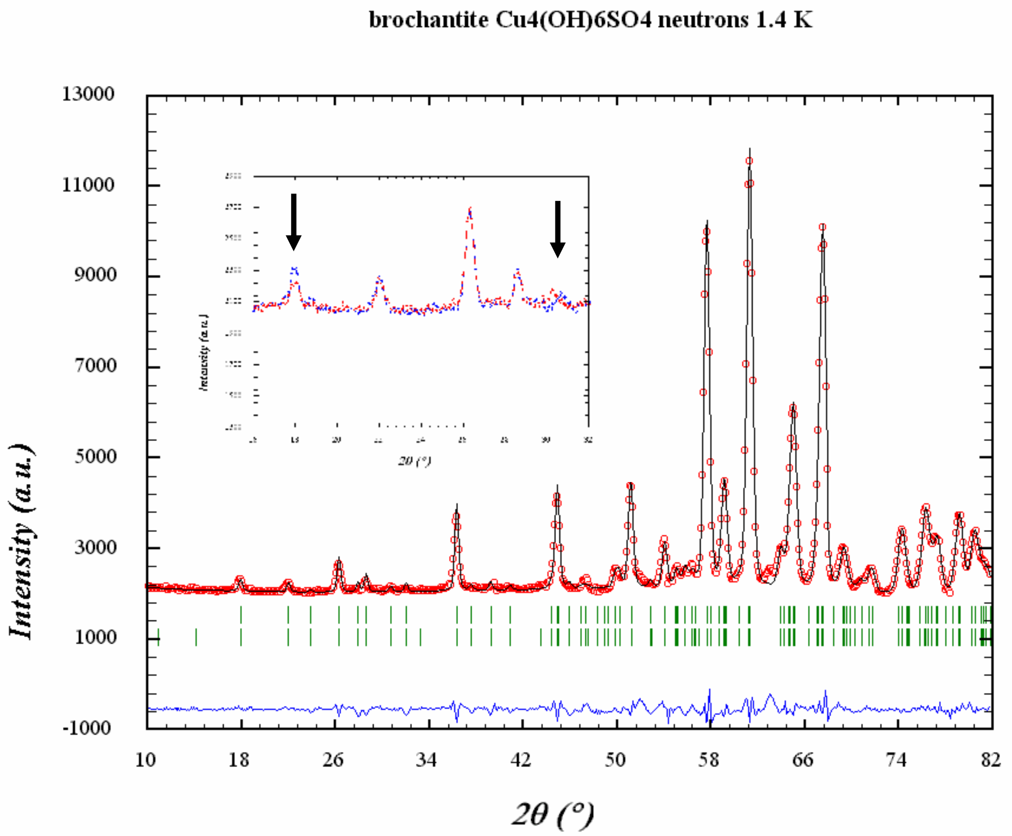

Figure S5. Observed (O) and calculated (——) profiles of the neutron pattern of $Cu_4(OH)_6SO_4$ obtained on the G4.1 diffractometer at 1.4 K with position of the Bragg reflections (short vertical lines, nuclear, magnetic) and difference between observed and calculated profiles. Inset : Zoom in the 16 to 32° region for the 1.4 K (blue) and 12 K (red) data, the arrows evidencing the magnetic contributions at 18 and 30.7°.

Table S1. Fractional atomic positions and isothermal temperature factors from neutron powder diffraction data at 300 K for deuterated brochantite.

Atom	x/a	y/b	z/c	B (Å^2)	Occupancy
Cu1	0.2942(7)	0.4889(8)	0.5297(17)	0.84(13)	4.0
Cu2	0.2940(8)	0.4938(10)	1.0210(21)	0.82(15)	4.0
Cu3	0.1168(6)	0.2558(10)	0.1788(17)	0.91(13)	4.0
Cu4	0.1192(7)	0.2579(10)	0.6867(20)	0.83(13)	4.0
S	0.3936(12)	0.1824(13)	0.3330(44)	0.90(24)	4.0
OH1	0.0970(10)	0.1333(12)	0.4297(26)	0.86(20)	4.0
OH2	0.0867(9)	0.1299(12)	0.9189(25)	0.99(18)	4.0
OH3	0.1582(11)	0.3826(13)	0.4571(27)	1.14(23)	4.0
OH4	0.1590(9)	0.3871(11)	0.9385(21)	1.23(20)	4.0
OH5	0.2488(8)	0.5940(10)	0.2538(31)	1.52(16)	4.0
OH6	0.3625(7)	0.3932(10)	0.8139(28)	1.33(15)	4.0
O1	0.2870(11)	0.1459(11)	0.2700(41)	2.87(22)	4.0
O2	0.3809(8)	0.3433(9)	0.3158(31)	2.08(17)	4.0
O3	0.4446(13)	0.1452(17)	0.0807(33)	3.11(30)	4.0
O4	0.4441(11)	0.1549(14)	0.5431(19)	2.43(17)	4.0
D1	0.0226(12)	0.1056(15)	0.3840(34)	2.51(24)	4.0
D2	0.0137(9)	0.1096(12)	0.8902(23)	1.24(18)	4.0
H3	0.1060(11)	0.4581(12)	0.4277(29)	1.39(21)	0.17(8)
D3	0.1060(11)	0.4581(12)	0.4277(29)	1.39(21)	3.83(8)
H4	0.1066(14)	0.4468(14)	0.9118(31)	2.11(27)	0.26(8)
D4	0.1066(14)	0.4468(14)	0.9118(31)	2.11(27)	3.74(8).
D5	0.1714(8)	0.5995(10)	0.2232(30)	2.25(16)	4.0
H6	0.3443(9)	0.3068(11)	0.8081(31)	1.57(19)	0.46(5)
D6	0.3443(9)	0.3068(11)	0.8081(31)	1.57(19)	3.54(5)

D/(H+D) = 0.96

Table S2. Interatomic distances (Å) and angles (°) for deuteriated brochantite from neutron data at 300 K.

Cu1-OH1	1.99(2)	OH1-Cu1-OH3	165(6)	OH3-Cu1-O2	94.5(10)
Cu1-OH3	2.03(2)	OH1-Cu1-OH5	78.0(10)	OH5-Cu1-OH6	171(10)
Cu1-OH5	1.93(2)	OH1-Cu1-OH6	93.8(10)	OH5-Cu1-O1	90.2(13)
Cu1-OH6	1.98(2)	OH1-Cu1-O1	82.2(9)	OH5-Cu1-O2	87.0(8)
Cu1-O1	2.36(2)	OH1-Cu1-O2	94.5(9)	OH6-Cu1-O1	92.1(10)
Cu1-O2	2.39(2)	OH3-Cu1-OH5	90.6(11)	OH6-Cu1-O2	90.3(11)
<Cu1-O>	2.11	OH3-Cu1-OH6	98.0(12)	O1-Cu1-O2	176(10)
		OH3-Cu1-O1	88.3(10)		
Cu2-OH2	2.03(2)	OH2-Cu2-OH4	170(9)	OH4-Cu2-O2	95.7(10)
Cu2-OH4	2.02(2)	OH2-Cu2-OH5	83.5(9)	OH5-Cu2-OH6	171(10)
Cu2-OH5	1.92(2)	OH2-Cu2-OH6	90.0(10)	OH5-Cu2-O1	93.2(14)
Cu2-OH6	1.97(2)	OH2-Cu2-O1	84.8(11)	OH5-Cu2-O2	87.2(9)
Cu2-O1	2.36(2)	OH2-Cu2-O2	93.6(9)	OH6-Cu2-O1	92.4(10)
Cu2-O2	2.39(2)	OH4-Cu2-OH5	92.6(11)	OH6-Cu2-O2	87.1(11)
<Cu2-O>	2.12	OH4-Cu2-OH6	94.8(10)	O1-Cu2-O2	178(10)
		OH4-Cu2-O1	86.0(10)		
Cu3-OH1	2.00(2)	OH1-Cu3-OH2	100.6(13)	OH2-Cu3-O3	93.2(11)
Cu3-OH2	1.97(2)	OH1-Cu3-OH3	78.9(7)	OH3-Cu3-OH4	97.2(11)
Cu3-OH3	2.06(2)	OH1-Cu3-OH4	172(10)	OH3-Cu3-O1	91.8(10)
Cu3-OH4	2.11(2)	OH1-Cu3-O1	80.4(9)	OH3-Cu3-O3	90.5(11)
Cu3-O1	2.43(2)	OH1-Cu3-O3	98.7(12)	OH4-Cu3-O1	93.2(10)
Cu3-O3	2.41(2)	OH2-Cu3-OH3	176(10)	OH4-Cu3-O3	87.9(10)
<Cu3-O>	2.16	OH2-Cu3-OH4	82.9(8)	O1-Cu3-O3	177(10)
		OH2-Cu3-O1	84.4(10)		
Cu4-OH1	1.95(2)	OH1-Cu4-OH2	98.2(12)	OH2-Cu4-O4	97.8(10)
Cu4-OH2	2.00(2)	OH1-Cu4-OH3	81.5(9)	OH3-Cu4-OH4	94.1(11)
Cu4-OH3	2.00(2)	OH1-Cu4-OH4	173(10)	OH3-Cu4-OH5	103.4(11)
Cu4-OH4	1.96(2)	OH1-Cu4-OH5	69.8(8)	OH3-Cu4-O4	84.7(10)
Cu4-OH5	2.33(1)	OH1-Cu4-O4	89.1(10)	OH4-Cu4-OH5	106.0(11)
Cu4-O4	2.42(2)	OH2-Cu4-OH3	177(10)	OH4-Cu4-O4	96.1(10)
<Cu4-O>	2.11	OH2-Cu4-OH4	85.9(9)	OH5-Cu4-O4	156(3)
		OH2-Cu4-OH5	74.2(7)		
Cu1-Cu2	2.96(2)	Cu3-Cu4	2.97(2)	Cu1-Cu2-Cu1	178(10)
Cu1-Cu2	3.07(2)	Cu3-Cu4	3.06(2)	Cu3-Cu4-Cu3	179(10)

Table S3. Atomic positions from neutron powder data at 1.4 K for deuteriated brochantite.

Atom	x/a	y/b	z/c	Mx (μ_B)	Occupancy
Cu1	0.289(1)	0.488(2)	0.522(4)	0.22(11)	4.0
Cu2	0.303(1)	0.495(1)	1.037(3)	0.22(11)	4.0
Cu3	0.126(1)	0.264(1)	0.186(4)	0.74(7)	4.0
Cu4	0.118(1)	0.253(2)	0.661(3)	0.74(7)	4.0
S	0.386(4)	0.184(4)	0.313(13)		4.0
OH1	0.099(2)	0.123(3)	0.409(5)		4.0
OH2	0.090(2)	0.119(3)	0.898(5)		4.0
OH3	0.178(2)	0.399(3)	0.471(5)		4.0
OH4	0.177(2)	0.383(3)	0.991(5)		4.0
OH5	0.246(2)	0.602(2)	0.234(4)		4.0
OH6	0.384(1)	0.396(2)	0.804(5)		4.0
O1	0.279(2)	0.134(2)	0.261(5)		4.0
O2	0.371(1)	0.343(2)	0.304(5)		4.0
O3	0.460(2)	0.146(2)	0.166(3)		4.0
O4	0.440(2)	0.153(2)	0.573(5)		4.0
H1	0.007(2)	0.095(2)	0.386(5)		0.05(8)
D1	0.007(2)	0.095(2)	0.386(5)		3.95(8)
D2	0.006(2)	0.136(2)	0.895(4)		4.0
D3	0.097(2)	0.454(3)	0.463(5)		4.0
H4	0.111(1)	0.442(3)	0.923(6)		0.17(8)
D4	0.111(1)	0.442(3)	0.923(6)		3.83(8).
D5	0.132(1)	0.603(1)	0.178(5)		4.0
H6	0.325(1)	0.296(2)	0.754(5)		0.30(6)
D6	0.325(1)	0.296(2)	0.754(7)		3.70(6)

Table S4. Atomic positions and magnetic moment of the copper atoms within the cell at 1.4K.

Atom	x/a	y/b	z/c	M_x (μ_B)
Cu11	0.289(1)	0.488(2)	0.522(4)	0.22(11)
Cu12	0.711	0.512	0.478	-0.22(11)
Cu13	0.211	0.988	0.478	0.22(11)
Cu14	0.789	0.012	0.522	-0.22(11)
Cu21	0.303(1)	0.495(1)	1.037(3)	0.22(11)
Cu22	0.697	0.505	-0.037	-0.22(11)
Cu23	0.197	0.995	-0.037	0.22(11)
Cu24	0.803	0.005	1.037	-0.22(11)
Cu31	0.126(1)	0.264(1)	0.186(4)	-0.74(7)
Cu32	0.874	0.736	0.814	0.74(7)
Cu33	0.374	0.764	0.814	-0.74(7)
Cu34	0.626	0.236	0.186	0.74(7)
Cu41	0.118(1)	0.253(2)	0.661(3)	-0.74(7)
Cu42	0.882	0.747	0.339	0.74(7)
Cu43	0.382	0.753	0.339	-0.74(7)
Cu44	0.618	0.247	0.661	0.74(7)